In the first case, one input of the analyser is used to process the filter output node and the other constitutes the additional observation point. Obviously, this point has to be judiciously chosen to be able to obtain an increase in fault coverage. So, the two analyser inputs are connected to (i) the output node of the filter and (ii) the output node of the op-amp differential stage as shown in Fig. 2. The HSPICE fault simulations show that in this situation, only one fault is not detected. The corresponding fault coverage is equal to: FC_{AS} (V_{out} and V_{diff}) = 97.9%.

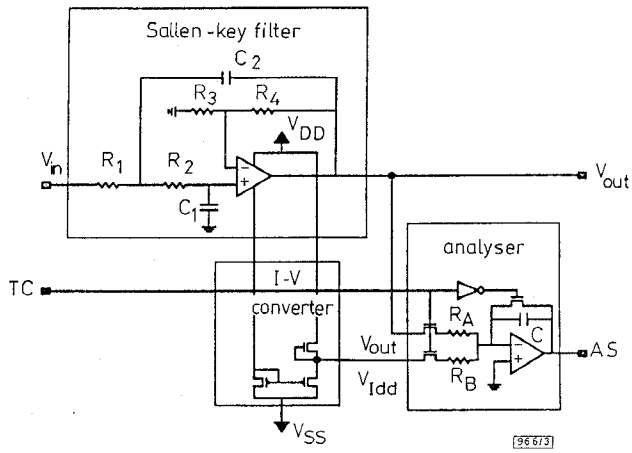

Fig. 3 *Mixed voltage/current testing*

In the second case, one input of the analyser is used to process the filter output and the other to observe the supply current. Since the analyser is designed for voltage integration, an additional subcircuit is required to provide a voltage V_{Idd}, which is an image of the supply current I_{dd} of the CUT. The two analyser inputs are then connected to (i) the output node V_{out} of the filter and (ii) the output node V_{Idd} of the I-V converter. as illustrated in Fig. 3. The I-V converter we use is based on work related in [7] to the area of current sensor development. Fault simulation results show that this structure allows us to detect 47 of the 48 faults for the filter. The resulting fault coverage is equal to: FC_{AS} (V_{out} and I_{dd}) = 97.9%.

So in both cases, we can observe a significant increase in the fault coverage achieved when compared to a classical time-domain analysis: from 85.4% up to 97.9%. This improvement in circuit testability is achieved while maintaining a reasonable area overhead since a single opamp is required to build the analogue signature. Furthermore, it has to be emphasised that usually, when using signature analysis techniques, the problem is to minimise the number of error masking phenomena in order to obtain a fault coverage as close as possible to the fault coverage achieved by an external test. With the multiple-input analogue analyser, not only can we partially overcome aliasing problems by introducing redundancy, but also we gain an improvement in fault coverage. This solution consequently goes beyond the classical objectives of signature analysis techniques.

Conclusion: Based on the use of the integration function as an analogue compaction technique, we have proposed a system for deriving a signature for analogue circuits. A signature analyser can therefore be defined and easily implemented using an on-chip opamp-based integrator. This permits us to replace the hard-to-manage external monitoring of a continuous time-varying response by a simple single-shot analogue measurement. Furthermore, the ability of our multiple-input analyser to concurrently monitor different internal test points allows us to partly overcome the aliasing problem and to improve circuit testability. It is shown that by using multiple-node voltage testing, we can drastically increase the fault coverage achieved for a Sallen-key filter. Also, it is shown that our system allows the implementation of concurrent control of both voltage and current levels, thus allowing us to fully profit from the complementarity between voltage and I_{ddq} test techniques.

4 October 1996
Electronics Letters Online No: 19961511

M. Renovell, F. Azaïs and Y. Bertrand (*Laboratoire d'Informatique, Robotique et Microélectronique de Montpellier (LIRMM), UMR 55506, Université de Montpellier II/CNRS, 161, Rue Ada, 34392 Montpellier Cedex 5, France*)

References

1 ABRAMOVICI, M., BRAUER, M.A., and FRIEDMAN, A.D.: 'Digital systems testing and testable designs' (Computer Science Press, New York, 1995)
2 RAJSKI, J., and TYSZER, J.: 'The analysis of digital integrators for test response compaction', *IEEE Trans. Circuits Syst. II*, 1992, pp. 293–301
3 OHLETZ, M.J.: 'Hybrid built-in self-test (HBIST) for mixed analogue/digital integrated circuits'. Proc. European Test Conf., 1991, pp. 307–316
4 NAGI, N., CHATTERJEE, A., and ABRAHAM, J.A.: 'A signature analyzer for analog and mixed-signal circuits'. Proc. Int. Conf. Comput.-Aided-Des., 1994, pp. 284–287
5 BELL, I.M., CAMPLIN, D.A., TAYLOR, G.E., and BANNISTER, B.R.: 'Supply current testing of mixed analogue and digital ICs', *Electron. Lett.*, 1991, **27**, (17). pp. 1581–1583
6 MACHADO DA SILVA, J., MATOS, J.S., BELL, I.M., and TAYLOR, G.E.: 'Cross correlation between I_{dd} and V_{out} signals for testing analog circuits', *Electron. Lett.*, 1995, **31**, (19), pp. 1617–1618
7 ROCA, M., and RUBIO, A.: 'Self testing CMOS operational amplifier', *Electron. Lett.*, 1992, **28**, (5), pp. 1452–1454

Perturbation of the Sierpinski antenna to allocate operating bands

C. Puente, J. Romeu, R. Bartolemé and R. Pous

Indexing terms: Antennas, Fractals, Antenna arrays

A scheme for modifying the spacing between the bands of the Sierpinski antenna is introduced. Experimental results of two novel designs of fractal antennas suggest that the fractal structure can be perturbed to enable the log-period to be changed while still maintaining the multiband behaviour of the antenna.

Introduction: The application of fractal structures to the design of antennas has been recently described [1 – 3]. In the Sierpinski antenna, presented in [2, 4], both the input and the radiation patterns have a log-periodic behaviour. The log-period (δ) had a factor of 2 (δ = 2), the same scale factor that characterised the geometrical self-similarity properties of the fractal object. Here, we describe some experimental results on two novel structures based on the Sierpinski gasket, which present different log-periods (δ = 1.66 and δ = 1.5). The results suggest a method for perturbing the Sierpinski structure in such a way as to control the position of multiple bands where necessary.

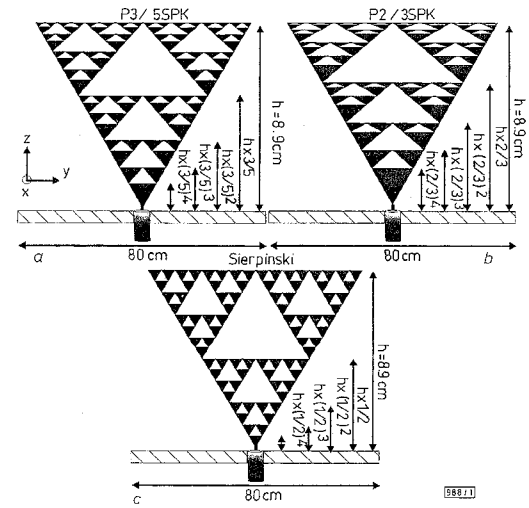

Fig. 1 *Two novel designs and original Sierpinski antenna*

a P3/5SPK antenna
b P2/3SPK antenna
c Original Sierpinski antenna

Design: The behaviour of the Sierpinski antenna has been explained through the existence of a current density active region

over a fractal surface [4]. Such an active region self-scales at each wavelength in an analogous way, which has been previously described for the log-periodic dipole array and for the spiral antenna [5]. That is, at short wavelengths, the current tends to concentrate towards the feeding point in a region where a small copy of the overall shape of the antenna is located. This region of the antenna has the most significant contribution to radiation and the rest of the antenna outside it becomes effectively disconnected. This Letter aims to show how, by perturbing the characteristic scale factor of the fractal shape, the radiating bands can be shifted.

The two novel designs are plotted in Fig. 1 together with the original Sierpinski antenna [2]. Both have the overall form replicated at five different scales at the base of the antenna, the smaller copy being a single triangle. The antennas are designed by means of an iterative algorithm that basically consists in subtracting a scaled triangle from the original triangular form [6]. At each iteration, a reduction factor of 3/5 is found on the lower triangular cluster of the first antenna (hereafter P3/5SPK) and a reduction factor of 2/3 is found on the second one (hereafter P2/3SPK). We note that the two upper triangular clusters that remain after each subtraction are not proportional copies of the overall shape but are rather distorted. An affine transformation rather than a similarity transformation should be applied to go from the overall structure to these skewed gaskets, and hence the form is said to be self-affine [6] instead of self-similar. Nevertheless, a similarity relation holds for the lower cluster where the active region is expected to be concentrated, and hence a self-similar electromagnetic behaviour can be expected for both structures.

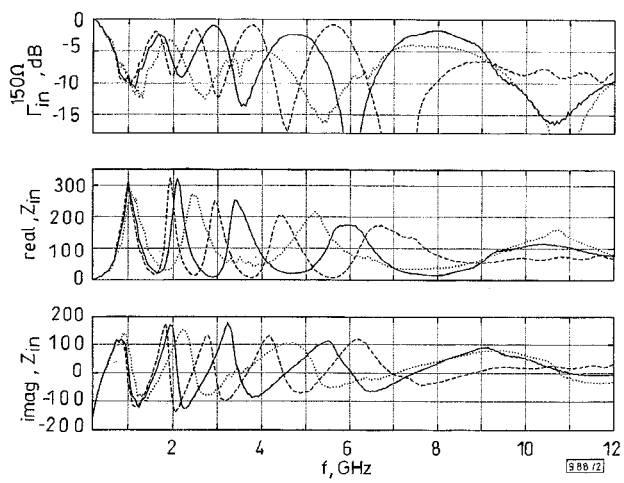

Fig. 2 *Input reflection coefficient relative to 150Ω ($\Gamma_{in}^{150\Omega}$), input resistance and reactance of three antennas*

——— P3/5SPK
– – – – P2/3SPK
····· Sierpinski

Experimental results: The antennas were printed over a Cuclad 250 dielectric substrate (ε_r = 2.5 and h = 1.588mm) using standard printed circuit techniques, and mounted on a monopole configuration over a 80 × 80cm square conductor ground plane. The antennas' input reflection coefficient relative to 50Ω were measured from 200MHz to 12GHz using an HP8510B. Such coefficients were renormalised with respect to 150Ω which is the impedance that better fits the antenna input impedance at each band (antiresonant frequencies). Such reflection coefficients ($\Gamma_{in}^{150\Omega}$) together with the real and imaginary parts of the input impedance (Z_{in}) are plotted in Fig. 2; the corresponding parameters for the previously reported Sierpinski antenna [4] are shown for comparison as well. To show the log-periodic behaviour of the three antennas, the resonant frequencies together with the spacing factor among them are listed in Table 1. The data display an almost log-periodic distribution of the upper bands with log-periods δ = 1.66 (5/3) for the P3/5SPK antenna and δ = 1.5 (3/2) for the P2/3SPK antenna, which are the scale factors that characterise their fractal body. The lower bands are shifted towards the origin due to the truncation effect and are closer to that of a bow-tie antenna as described in [4].

The patterns of the two novel designs were measured in an anechoic chamber at the centre of the four upper bands (Figs. 3 and 4).

Table 1: Band start frequencies (resonances) and scale factor between adjacent bands for the P3/5SPK, P2/3SPK and Sierpinski antennas

P3/5SPK		P2/3SPK		Sierpinski	
f_n	f_n/f_{n-1}	f_n	f_n/f_{n-1}	f_n	f_n/f_{n-1}
0.45	–	0.44	–	0.46	–
1.61	3.57	1.54	3.46	1.75	3.77
2.76	1.71	2.43	1.57	3.51	2.00
4.54	1.65	3.69	1.51	7.01	2.00
7.52	1.66	5.43	1.47	13.89	1.98

In general, the main cuts display a characteristic two lobe structure similar to the corresponding pattern of a monopole. The patterns keep a notable degree of similarity among bands with a slight increase of ripples at the highest bands, mainly due to the non-ideal behaviour of the ground plane. In general, the θ = 90° cut shows almost isotropic behaviour in that plane, with a slight tendency to enhance radiation in the direction perpendicular to the antennas' surface (such a feature was also apparent on the Sierpinski antenna). The multiband behaviour of the antennas, together with the shape of the patterns suggest a possible application of these designs to land vehicles linked to ground base-stations that might require the operation of several communication systems in a single antenna.

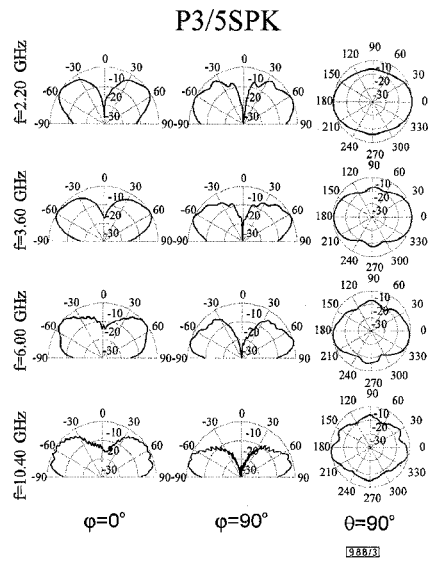

Fig. 3 *Main cuts (φ = 0°, φ = 90°, θ = 90°) of radiation patterns for P3/5SPK antenna*

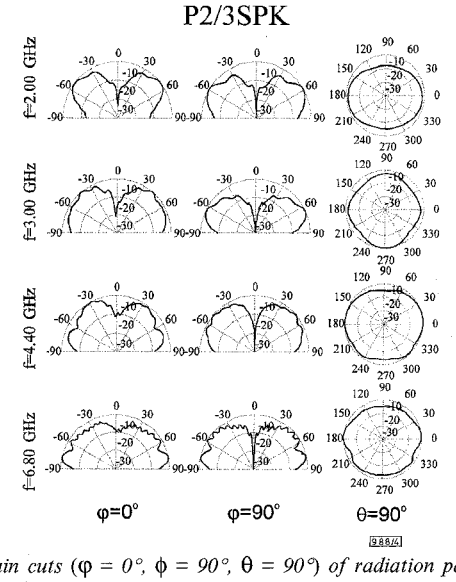

Fig. 4 *Main cuts (φ = 0°, φ = 90°, θ = 90°) of radiation patterns for P2/3SPK antenna*

Conclusions: Two novel designs of fractal multiband antennas have been introduced. The antennas were designed by perturbing the shape of the Sierpinski antenna. The spacing between bands is again related to the characteristic scale factor of the fractal structure, which suggests a procedure for tuning the antenna to a required set of bands. The multiband behaviour is consistent both from the input impedance and radiation pattern points of view.

Acknowledgments: The authors would like to thank P.Mayes from the University of Illinois for encouraging this work. They also thank A.Hijazo and M.Navarro for contributions on the antenna design and measurements. This work has been financially supported by the 'Spanish Commission of Science and Technology' under grant TIC-96-0724-C06-04.

7 October 1996
Electronics Letters Online No: 19961476

C. Puente, J. Romeu, R. Bartolemé and R. Pous (*D3-Electromagnetics and Photonics Engineering Group, Signal Theory and Communications Department, Universitat Politècnica de Catalunya, Gran Capità s/n, Mòdul D3, 08034 Barcelona, Spain*)

References

1 PUENTE, C., and POUS, R.: 'Fractal design of multiband and low side-lobe arrays', *IEEE Trans. Antennas Propag.*, 1996, **44**, (5), pp. 730–739
2 PUENTE, C., ROMEU, J., POUS, R., GARCIA, X., and BENÍTEZ, F.: 'Fractal multiband antenna based on the Sierpinski gasket', *Electron. Lett.*, 1996, **32**, (1), pp. 1–2
3 COHEN, N., and HOHLFELD, R.G.: 'Fractal loops and the small loop approximation', *Commun. Quarterly*, 1996, pp. 77–81
4 PUENTE, C., ROMEU, J., POUS, R., and CARDAMA, A.: 'On the behaviour of the Sierpinski multiband fractal antenna', *IEEE Trans. Antennas Propag.*, 1996, (Submitted)
5 RUMSEY, V.H.: 'Frequency independent antennas' (Academic Press, New York, 1966)
6 PEITGEN, H.O., JÜRGENS, H., and SAUPE, D.: 'Chaos and fractals, new frontiers of science' (Springer-Verlag, New York, 1992)

40Gbit/s OTDM soliton transmission over transoceanic distances

G. Aubin, T. Montalant, J. Moulu, F. Pirio, J.-B. Thomine and F. Devaux

Indexing terms: Soliton transmission, Time division multiplexing

40Gbit/s soliton transmission is achieved in a recirculating loop over 10000km, for the first time to the authors' knowledge, with a single carrier wavelength. Propagation has been tested with and without polarisation multiplexing thanks to low polarisation dependency electroabsorption modulators for in-line control and for the time demultiplexing receiver.

Introduction: Soliton transmission is an attractive candidate on which to base optical transoceanic systems although it requires in-line passive or active control to achieve high capacity over long distances [2]. Thanks to its nonlinear characteristic, it allows noise rejection out of the signal bandwidth. In particular, optical regeneration can be achieved by incorporating frequency filtering and in-line synchronous intensity modulation. This technique limits the increase in amplitude noise and timing jitter, allows transmission over unlimited distance [2] and a large repeater span [3]. It was shown to be possible by the simulation results in [4] and it is demonstrated here experimentally for the first time to our knowledge that 40Gbit/s transoceanic transmission can be achieved on a single carrier wavelength when the longest haul reported with periodic dispersion compensation is 5000km [5].

This method does not preclude the use of WDM transmission, as it has been demonstrated with a binary error rate (BER) of $< 10^{-8}$ at 10000km [6] and could be competitive with the sliding technique [7].

Experiment: The setup includes a 180km long recirculating loop operating as in our previously published experiments [3, 4] and is shown in Fig. 1.

Transmission has been tested with two different 40Gbit/s pulses transmitters. Adjacent pulse polarisation is orthogonal in one and parallel in the other.

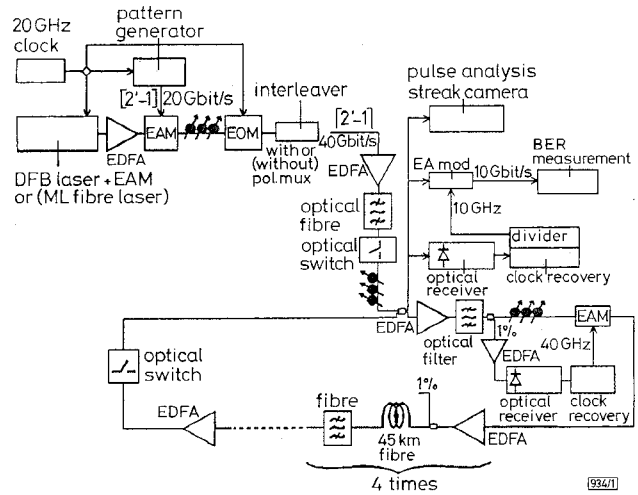

Fig. 1 *Experimental setup*

The first transmitter generates 20Gbit/s 2^7–1 pseudorandom pattern pulses from a 1.5572μm DFB laser and through two InGaAsP-InGaAsP multiquantum well (MQW) electroabsorption ridge modulators and an amplifier integrated on the same chip using a common active layer [8]. The short pattern length is limited by the electronic driver made in our laboratory. A second stage reshapes these pulses using a Mach-Zehnder lithium niobate optical intensity modulator driven at 20GHz. Optical time multiplexing is realised after splitting a 20Gbit/s stream. The pulse train is interleaved with itself after an adequate delay obtained using precise fibre length. A polarisation combiner provides orthogonal states between consecutive pulses with an extinction ratio > than 25dB.The output average pulsewidth measurement gives 17ps with a streak camera.

The second 1.5572μm source uses the same 20Gbit/s modulation but 20GHz pulses come by a mode-locked fibre ring laser instead of an electroabsorption modulator (EAM) and a DFB laser. An identical passive technique achieves 20–40Gbit/s optical multiplexing to provide 2^7–1 pseudorandom pattern. However, relative polarisation states are managed here in each branch of a conventional coupler in order to optimise the output alignment through the main axis of a polariser that maintains the same parallel polarisation for every launched pulses. The 7ps average pulsewidth is shorter than the previous one and better extinction allows us to transmit them without any residual interference beating.

The propagation path contains a modulation control section followed by four 45km long fibre spans. Loss compensation is realised by 980nm pumped amplifying and filtering by an interferential device in each section. The loop experiment needs another amplifier to balance switch and coupler attenuation and to reach suitable powers. The average fibre input power measured through 99:1 couplers placed just in front of the 12.5dB loss fibre spools is then ~5dBm. The combination of in-line optical bandpass filters leads to a 0.77nm FWHM Gaussian shaped filtering per 180km. A short piece of 17ps/nm/ km step-index fibre has been spliced to dispersion-shifted fibres (DSF) in order to set the chromatic dispersion at 0.2ps/nm/km in each amplifying span. The resynchronising section comprises a high bandwidth optical receiver to recover the 40GHz clock straight from 40Gbit/s pulses and an EAM [9] driven by resulting 40GHz, 20dBm sinusoid to reshape in-line pulses with a total polarisation dependency loss (PDL) of < 1dB.

Straight 40 to 10Gbit/s demultiplexing is realised with another MQW EAM [9] driven sinusoidally at 10GHz with created subharmonics coming from a second 40GHz clock recovery device. The BER is measured after this optical time demultiplexing by using a 10Gbit/s commercial BER counter triggered with a delayed gate corresponding to the propagation distance. At the